Performance evaluation of a Scheimpflug stereocamera for particle image velocimetry

Weijun Zang and Ajay K. Prasad

We describe a novel stereocamera for particle image velocimetry (PIV) applications that incorporates the Scheimpflug condition that the object plane, lens plane, and image plane must be collinear. We examined the governing equations for this system using a computer-based sensitivity analysis to predict the accuracy of the in-plane and out-of-plane measurement. We evaluated the performance of the Scheimpflug PIV system with a three-dimensional uniform translation test. Results indicate that the Scheimpflug PIV stereocamera performs as expected. The larger off-axis angles possible with the Scheimpflug system can provide a higher accuracy in the out-of-plane component when compared with a translation PIV stereocamera. © 1997 Optical Society of America

Key words: Particle image velocimetry, Scheimpflug, stereocamera.

1. Introduction

There are two basic stereoscopic particle image velocimetry (PIV) systems: (1) the translation method and (2) the angular-displacement method (Fig. 1). The conventional translation stereoscopic PIV system can provide good accuracy[1] when applied to three-dimensional (3-D) flows. However, as shown by Prasad and Adrian[1] the relative error of the out-of-plane measurement to the in-plane measurement for a translation stereocamera is given by $2d_1/S$, where d_1 is the object distance and S is the separation between lens axes [see Fig. 1(a)]. Therefore one can reduce the error in the out-of-plane measurement by decreasing d_1/S, i.e., by increasing the off-axis angle θ. As shown in Fig. 1(a), θ is the angle between the symmetry plane of the stereocamera system (z axis) and the line OO' subtended by the center of the object to the center of the lens. The translation system requires the two camera axes to remain parallel to each other. Therefore a large θ implies that the lenses are operating at the outer limit of their specifications. Consequently, there is a restriction placed on the maximum possible θ owing purely to the design of the lens. Also, when a liquid flow is imaged, the existence of the liquid–air interface results in significant radial distortions of the particle image. Prasad and Jensen[2] have shown by computer modeling that both limitations can be removed by adoption of the angular-displacement configuration in conjunction with a liquid prism. The liquid prism allows each camera to view the object plane in an orthogonal manner, minimizing radial distortions. At the same time, because the lens axes are rotated inward, the mean angle subtended by the object to the lens is zero. Thus, even for large θ, the largest angle subtended by the outermost edge of the object to the lens is well within lens specifications [Fig. 1(b)]. Because the lenses are no longer operating at the extreme of their specification range, larger off-axis angles are possible with the angular-displacement system. Consequently, it is expected that the angular-displacement system can provide higher accuracy.

The Scheimpflug condition[3] must be enforced in the angular-displacement system, which requires the object plane, lens plane, and image plane to be collinear [Fig. 1(b)]. This condition, first presented by Scheimpflug,[3] ensures that a sharp image can be obtained at the image plane. A derivation of the Scheimpflug condition is provided by Prasad and Jensen.[2] As a result of the Scheimpflug condition, the image plane is no longer parallel to the lens plane [Fig. 1(b)]. Rather, the angle between the lens plane and the object plane is equal to θ, and there is an additional angle α between the lens plane and the image plane,

When this study was performed, the authors were with the Department of Mechanical Engineering, University of Delaware, Newark, Delaware 19716. W. Zang is now with the Department of Biological Engineering, Cornell University, Ithaca, New York 14853.

Received 19 August 1996; revised manuscript received 19 May 1997.

0003-6935/97/338738-07$10.00/0

such that $\tan\alpha = M\tan\theta$, where M is the magnification. The associated disadvantage is the nonuniform magnification at the image plane; however, this disadvantage can be compensated for by a correction procedure based on ray-tracing described here. Thus it is natural to ask if the Scheimpflug system can provide a higher accuracy compared with the translation system.

2. Error Analysis

As a result of recording and interrogating the two views from each camera, the inputs to the combination algorithm are (1) the coordinates, and (2) particle displacements at the image or film plane. Therefore all the errors should be derived in terms of these quantities. As shown in Fig. 2, let Δx, Δy, and Δz represent the physical displacement of a particle in the fluid under the coordinate system $\langle\hat{x}, \hat{y}, \hat{z}\rangle$; let ΔX and ΔY represent the displacement of the particle at the image or film plane under the coordinate system $\langle\hat{x}_f, \hat{y}_f, \hat{z}_f\rangle$ (in this coordinate system ΔZ is zero); let $\Delta x'$ and $\Delta y'$ represent the projected displacement of the particle at the object plane under the coordinate system $\langle\hat{x}, \hat{y}, \hat{z}\rangle$ [again, $\Delta z'$ is zero (Fig. 2)]. Following the same procedure as Prasad and Adrian,[1] we obtain

$$\Delta x = \frac{\Delta x_2'[(\mathbf{p}_1 + \mathbf{q}_1)\cdot\mathbf{x}] - \Delta x_1'[(\mathbf{p}_2 + \mathbf{q}_2)\cdot\mathbf{x}]}{(\mathbf{p}_1 + \mathbf{q}_1)\cdot\mathbf{x} - (\mathbf{p}_2 + \mathbf{q}_2)\cdot\mathbf{x}}, \quad (1)$$

$$\Delta y = \frac{\Delta y_1' + \Delta y_2'}{2} - \frac{\Delta z}{d_1}\frac{(\mathbf{p}_1 + \mathbf{q}_1)\cdot\mathbf{y} + (\mathbf{p}_2 + \mathbf{q}_2)\cdot\mathbf{y}}{2}, \quad (2)$$

$$\Delta z = \frac{d_1(\Delta x_1' - \Delta x_2')}{(\mathbf{p}_1 + \mathbf{q}_1)\cdot\mathbf{x} - (\mathbf{p}_2 + \mathbf{q}_2)\cdot\mathbf{x}}, \quad (3)$$

$$(\mathbf{p}_1 + \mathbf{q}_1)\cdot\mathbf{x} - (\mathbf{p}_2 + \mathbf{q}_2)\cdot\mathbf{x} = S + \Delta x_1' - \Delta x_2'. \quad (4)$$

Because the interrogation process provides only the coordinates of a point ${x_f}^i$, ${y_f}^i$ and ΔX and ΔY at the image or film plane, we have to find $\Delta\mathbf{x}_i' \sim f(\Delta\mathbf{X}_i, \mathbf{x}_f{}^i)$, where $i = 1, 2$ for cameras 1 and 2, respectively. We begin by mapping a point ${x_f}^i$, ${y_f}^i$ at the film plane under the coordinate system $\langle\hat{x}_f, \hat{y}_f, \hat{z}_f\rangle$ to the corresponding coordinates x, y under the coordinate system $\langle\hat{x}, \hat{y}, \hat{z}\rangle$ at the object plane (Fig. 2). Following the ray-tracing principle, we have

$$\Delta x_i' = \frac{{x_f}^i\cos(\theta_b - \theta)z_3}{\cos(\theta)[{x_f}^i\cos(\theta_b - \theta)\tan(\theta) + {x_f}^i\sin(\theta_b - \theta) + c_2]} + \frac{({x_f}^i + \Delta X_i)\cos(\theta_b - \theta)z_3}{\cos(\theta)[{x_f}^i + \Delta X_i)\cos(\theta_b - \theta)\tan(\theta) + ({x_f}^i + \Delta X_i)\sin(\theta_b - \theta) + c_2]}, \quad (5)$$

$$\Delta y_i' = -\frac{z_3\Delta Y_i}{{x_f}^i\cos(\theta_b - \theta)\tan(\theta) + {x_f}^i\sin(\theta_b - \theta) + c_2}, \quad (6)$$

$$\Delta z_i' = 0, \quad (7)$$

where θ_b is the angle between the film plane and the object plane, θ is the angle between the lens plane and the object plane, and c_2 is the distance from the center of the lens to the center of the film plane. Combining Eqs. (1)–(7), one can obtain the expressions for real displacement. For the simplest case we assume that (1) $M = 1$ so $\theta_b = 2\theta$ and (2) the particle is at $x = y = z = 0$ during first exposure. Consequently, ${x_f}^i = {y_f}^i = 0$. Thus the following compact expressions are obtained:

$$\Delta x = \frac{S/2\left[-\frac{\Delta X_1 z_3}{2\Delta X_1\sin(\theta) + c_2} - \frac{\Delta X_2 z_3}{2\Delta X_2\sin(\theta) + c_2}\right]}{S + \frac{\Delta X_2 z_3}{2\Delta X_2\sin(\theta) + c_2} - \frac{\Delta X_1 z_3}{2\Delta X_1\sin(\theta) + c_2}}, \quad (8)$$

$$\Delta y = -\frac{z_3(\Delta Y_1 + \Delta Y_2)}{2c_2}\left(\frac{\Delta z}{d_1} - 1\right), \quad (9)$$

$$\Delta z = \frac{d_1\left[\frac{\Delta X_2 z_3}{2\Delta X_2\sin(\theta) + c_2} - \frac{\Delta X_1 z_3}{2\Delta X_1\sin(\theta) + c_2}\right]}{S + \frac{\Delta X_2 z_3}{2\Delta X_2\sin(\theta) + c_2} - \frac{\Delta X_1 z_3}{2\Delta X_1\sin(\theta) + c_2}}, \quad (10)$$

where d_1 is the object distance and S is the distance between the two lens centers. Following the standard procedure for error analysis, one can evaluate the error in the fluid displacement in terms of the errors in the measured displacement at the film plane and the PIV system parameters. Among all the parameters only θ, z_3, and c_2 are independent [see Fig. 1(b)]. Other parameters like d_1, S, and M can be deduced from them. In the present case z_3 and c_2 were set to 240 mm, which gives $M = 1$, the case considered for the sensitivity analysis as well as the uniform translation test. Let $\sigma_{\Delta X}$ denote the rms error in the measurement of the particle displacement at the film plane arising during PIV interrogation. As described in Prasad *et al.*[4] and Boillot and Prasad,[5] $\sigma_{\Delta X}$ is a cumulative error accruing from several sources, such as random errors caused by noise during recording and interrogation of PIV images,

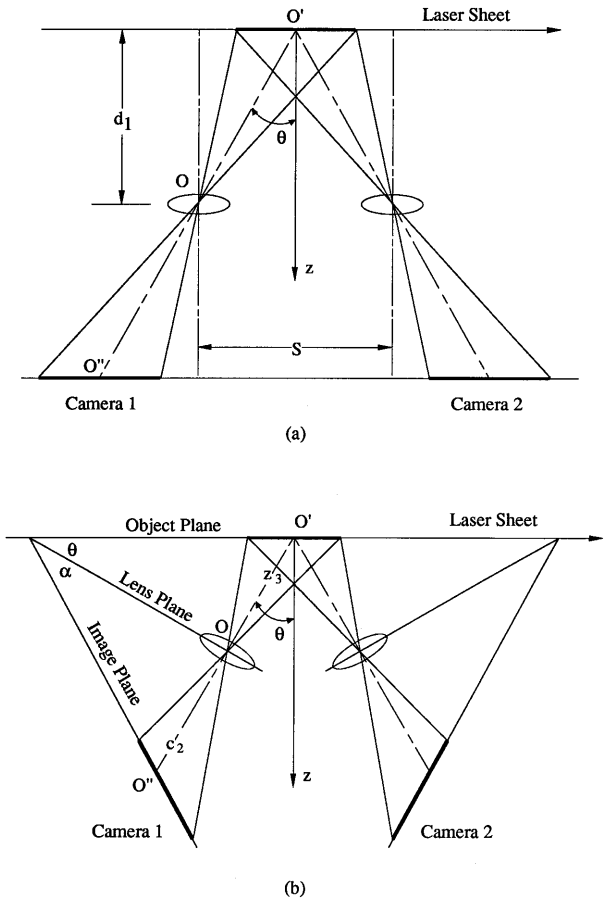

Fig. 1. Configurations for the (a) translation and (b) angular-displacement stereoscopic systems.

bias errors caused by the choice of correlation-peak detection scheme, and gradient errors caused by rotation and deformation of the flow within the interrogation spot. Because the same error mechanisms operate equally in X and Y, one can write $\sigma_{\Delta X} = \sigma_{\Delta Y}$. The error analysis in Appendix A lists the error in the 3-D fluid velocities $\sigma_{\Delta x}$, $\sigma_{\Delta y}$, and $\sigma_{\Delta z}$ in terms of $\sigma_{\Delta X}$. In other words, we normalize the rms error in the actual 3-D fluid velocities by the rms error arising during PIV interrogations only. The variations of $\sigma_{\Delta x}/\sigma_{\Delta X}$, $\sigma_{\Delta y}/\sigma_{\Delta X}$, and $\sigma_{\Delta z}/\sigma_{\Delta X}$ as a function of θ are plotted in Fig. 3. Here, again, we take the simplest case: ${x_f}^i = {y_f}^i = 0$, where $i = 1, 2$. Using the expressions for $\sigma_{\Delta x}$, $\sigma_{\Delta y}$, and $\sigma_{\Delta z}$ listed in Appendix A, one can obtain the curves shown in Fig. 3.

As seen in Fig. 3, a sharp decrease in $\sigma_{\Delta z}$ is found when θ increases from 0° to 10°. After that the rate of decrease slows down, although $\sigma_{\Delta z}$ decreases as θ is increased continuously. The variations in $\sigma_{\Delta x}$ and $\sigma_{\Delta y}$ are negligibly small. In fact, to a good approximation $\sigma_{\Delta x}/\sigma_{\Delta X} \approx \sigma_{\Delta y}/\sigma_{\Delta X} \approx 1/\sqrt{2}$; all this means is that the in-plane rms errors are reduced by $\sqrt{2}$ because we have two contributing measurements for the in-plane displacement instead of one. This gives us a good guide for the choice of θ: Increasing the angle provides diminishing returns after a certain value. If errors in x, y, S, M, and d_1 are neglected for the translation system and $M = 1$ the results predicted by Prasad and Adrian[1] can be rewritten as

$$\sigma_{\Delta z}/\sigma_{\Delta X} \approx 1/[\sqrt{2}\tan(\theta)], \tag{11}$$

$$\sigma_{\Delta x}/\sigma_{\Delta X} \approx 1/\sqrt{2}, \tag{12}$$

$$\sigma_{\Delta y}/\sigma_{\Delta X} \approx 1/\sqrt{2}. \tag{13}$$

In Fig. 3 all three error terms show behavior that is virtually identical to Eqs. (11)–(13). This is to be expected because we have presented an error analysis for ${x_f}^i = {y_f}^i = 0$. It is, however, reassuring to note the close match between our current error analysis and the one for the translation system derived earlier.[1] From Fig. 3 it appears that, as $\theta \to 0°$, the relative out-of-plane error becomes very large. This result is to be expected: In the limit of $\theta \to 0°$, the Scheimpflug system degenerates to a single camera oriented orthogonally to the object plane. In this situation the out-of-plane error becomes infinite, because we are, in fact, not able to resolve the out-of-plane component at all.

Based on Fig. 3, standard deviations of velocities in 3-D can be obtained for any desired angle; we selected $\theta = 20°$ for our uniform translation test. For the case of $\theta = 20°$, $M = 1$, and $z_3 = 240$ mm, the sensitivity analysis predicts that $\sigma_{\Delta z}/\sigma_{\Delta X} = 1.94$ and $\sigma_{\Delta x}/\sigma_{\Delta X} = 0.71$. So the ratio of the out-of-plane error to the in-plane error $\sigma_{\Delta z}/\sigma_{\Delta x}$ is predicted to be 2.75.

3. Uniform Translation Test

A. Experiment Hardware

To evaluate the performance of the Scheimpflug system, it is convenient for one to use a fluid flow wherein the velocity at each point is exactly known *a priori*. However, it is difficult to control the velocities precisely throughout the whole field in a real flow. Therefore, we designed an artificial flow simulating a uniform 3-D velocity field, as described by Prasad and Adrian[1] and Prasad *et al.*[4] To make each step of the recording process similar to an actual measurement, we used real particles to produce the test photographs.

We glued black carbospheres with a diameter of 30 μm to a piece of glass. The concentration of particles was approximately 10 particles/mm^2. Next a contact print of the glass plate was taken on Kodak Technical Pan 4415 film (10 cm × 12.5 cm), producing bright spots on a dark background. The contact print was sandwiched between two pieces of glass and mounted on a 3-D translation stage. By translating the stage, we obtained a precisely controlled movement. In the present case movements in only x and z directions were introduced while y was kept fixed. The contact print was backlit by a 60-W white lightbulb; to obtain evenly distributed light, we inserted a diffuser consisting of a thin sheet of white paper between the object plane and the light source. The PIV stereocamera used two identical Nikkor ED 120-mm F5.6 lenses (Nikon, Inc.). The system pa-

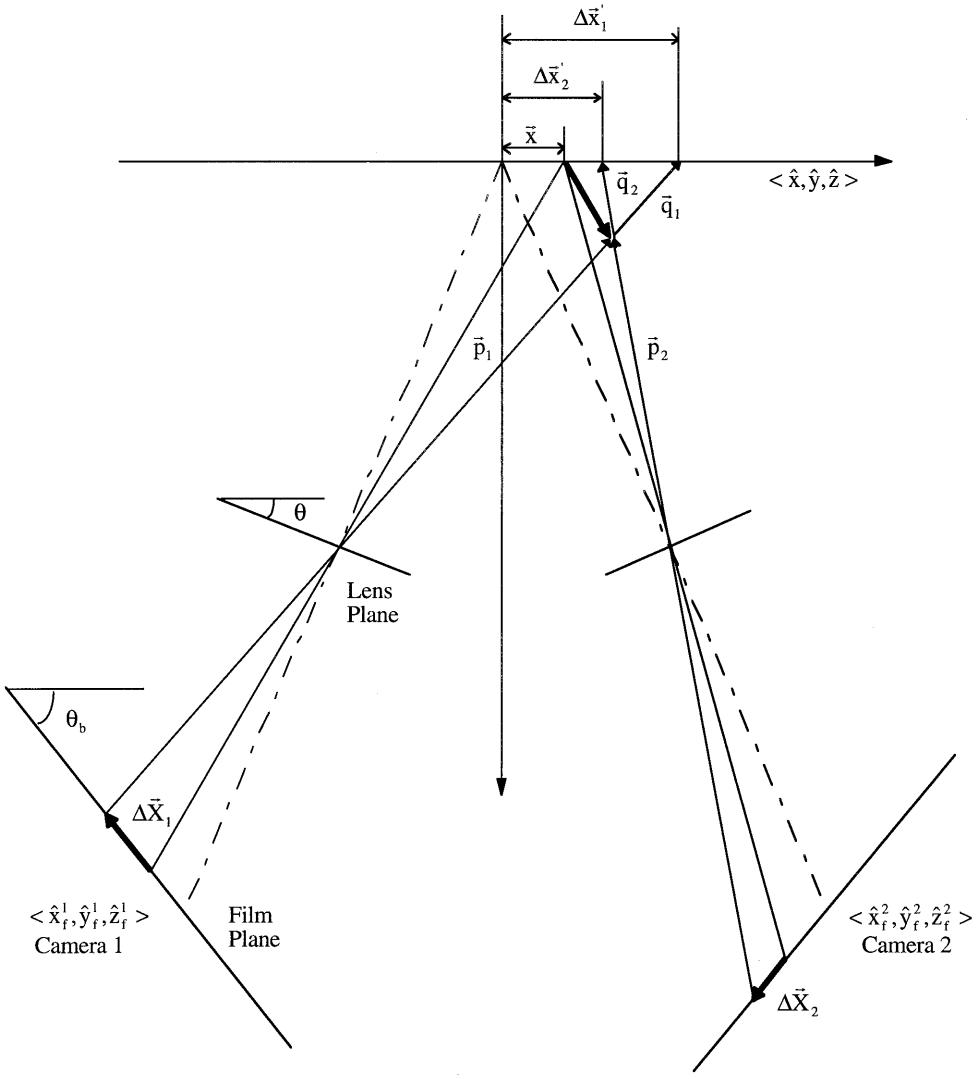

Fig. 2. Schematic of the Scheimpflug stereoscopic PIV system.

rameters were $\theta = 20°$, $\theta_b = 40°$, $c_2 = z_3 = 240$ mm, and $S = 164.17$ mm. For simplicity, no liquid–air interface was considered. Thus we obtained $M = 1$ at the center of the film plane. Other parts of the film plane were stretched in a nonuniform manner,

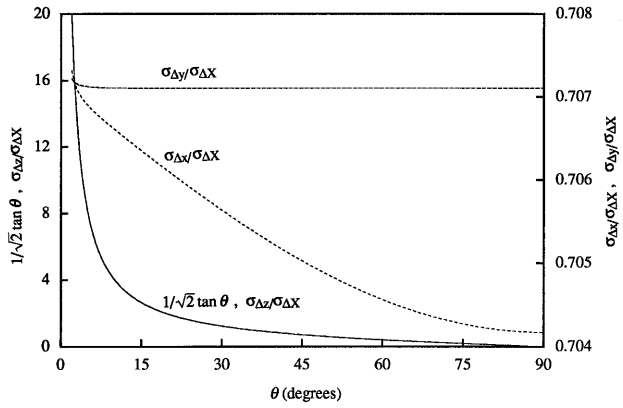

Fig. 3. Error analysis for 3-D displacement.

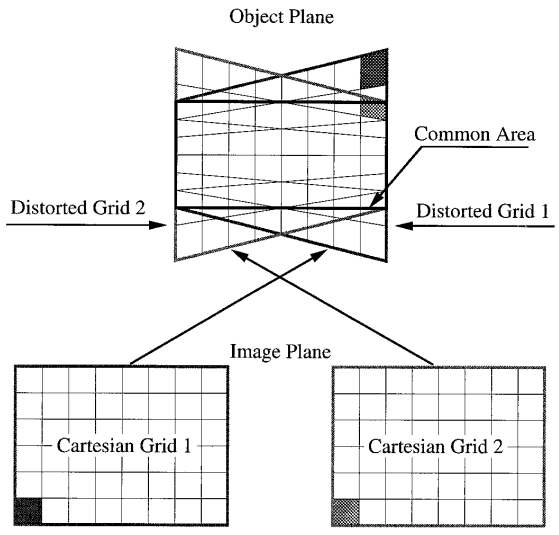

Fig. 4. Distorted view of the field from two cameras in the Scheimpflug system.

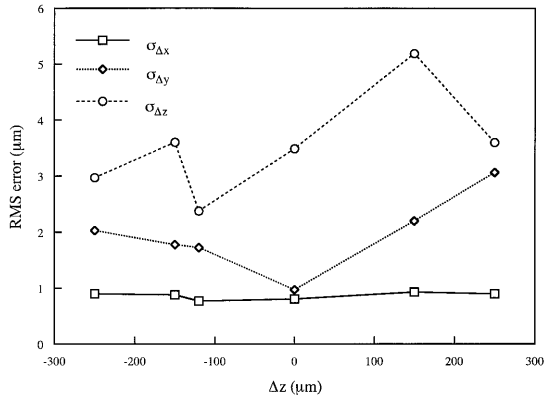

Fig. 5. RMS error in measured displacements for various Δz.

as depicted in Fig. 4. Considering the depth of field and diffraction effects,[6] we selected an *f*-number of 8. An exposure time of 2 s was optimal for Kodak TMAX400 film. The film was exposed twice: once before and once after the 3-D translation.

B. Image Interrogation System

The double-exposed film was digitized by a Nikon Coolscan digitizer (Nikon, Inc.) at a resolution of 106 dots/mm. The digitized image (18.8 mm × 28.2 mm) was processed with a resolution of 256 pixels × 256 pixels by the cross-correlation method described in detail by Boillot and Prasad.[5] We used a parabolic fit to locate the signal peak to subpixel accuracy. The following information was obtained from this step: coordinates and particle displacements at each grid point on the film plane under the coordinate system $\langle \hat{x}_f, \hat{y}_f, \hat{z}_f \rangle$.

Subsequently, we used a combining program to reconstruct the 3-D velocities from the data of these two cameras. The two rectangular interrogated domains from each camera are differentially stretched when mapped onto the object plane. As shown in Fig. 4, the two shaded regions are not only stretched differently but are also not coincident on the object plane. We overcame this effect of nonuniform magnification by adopting the following procedure: First, we mapped both the rectangular interrogated domains $\langle \hat{x}_f^1, \hat{y}_f^1, \hat{z}_f^1 \rangle$ and $\langle \hat{x}_f^2, \hat{y}_f^2, \hat{z}_f^2 \rangle$ to the object plane by use of the ray-tracing technique. Next, we determined the area common to these two distorted fields, and we superposed a square grid on it. We set the grid spacing equal to the largest grid spacing in the distorted field to eliminate a spurious increase in resolution. Third, we mapped the new, common, regular grid back to each film plane. Not surprisingly, they were themselves distorted in this process. We conducted bicubic-spline interpolation to interpolate the particle-displacement data from the original Cartesian grid of the film plane onto the distorted grid. Finally, we mapped the interpolated displacement vector back to the object plane. We could now

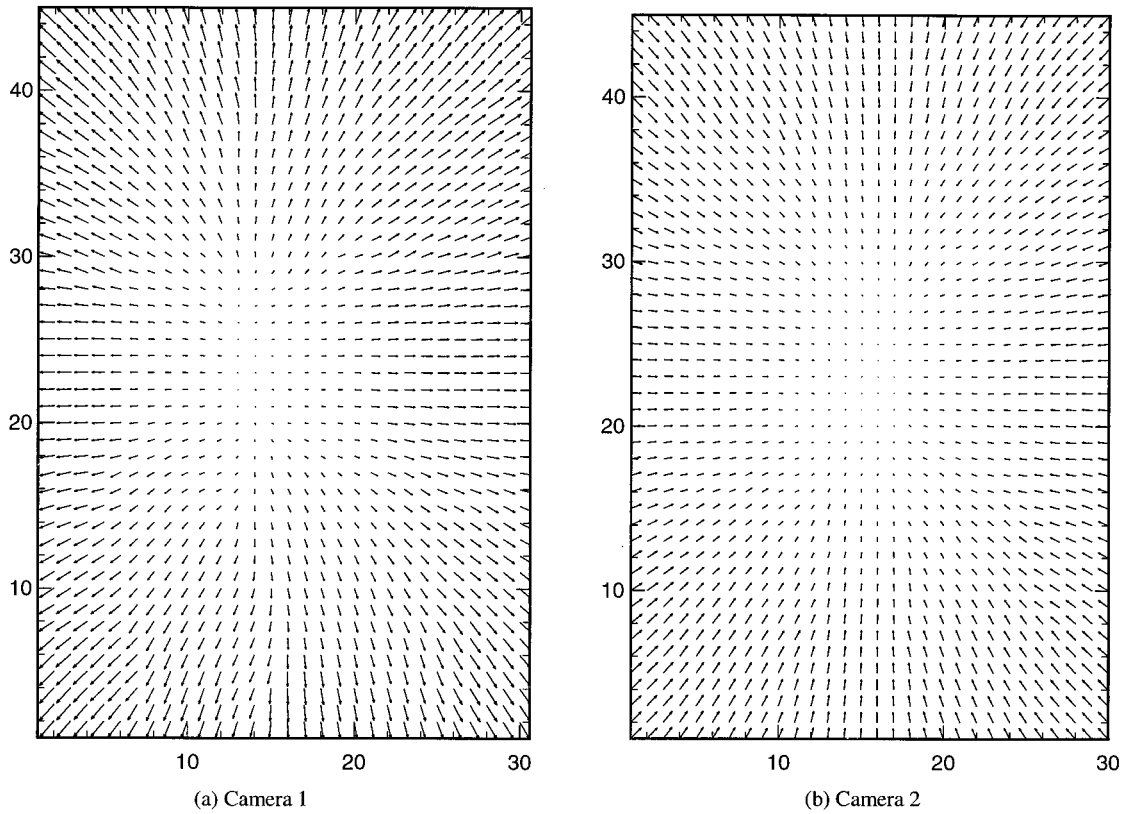

Fig. 6. Vector map from (a) camera 1 and (b) camera 2 for the case $\Delta x = -0.25$ mm, $\Delta y = 0$ mm, $\Delta z = -0.25$ mm; average displacements ($\langle \Delta X_1 \rangle = 0.34$ mm, $\langle \Delta Y_1 \rangle = 8.48 \times 10^{-4}$ mm; $\langle \Delta X_2 \rangle = 0.17$ mm, $\langle \Delta Y_2 \rangle = 4.1 \times 10^{-4}$ mm) have been subtracted from each vector.

combine the data from each camera using Eqs. (8)–(10).

C. Results

We obtained six groups of results. Figure 5 shows the rms error as a function of Δz. For the present case Δx was set to 250 μm, Δy was set to 0, and Δz was varied from −250 to 250 μm with the step of 125 μm. The case for $\Delta z = -150$ μm is different in that Δx was set to −200 μm. To detect invalid vectors, we found it essential to view the interrogated vector fields after subtracting the mean values $\langle \Delta X \rangle$ and $\langle \Delta Y \rangle$ from each vector; then the distribution of vectors could be seen more clearly (Fig. 6). Generally speaking, less than 1% of the vectors were invalid. For the six test cases the average ratio of out-of-plane error to in-plane error $\sigma_{\Delta z}/\sigma_{\Delta x}$ is 3.53, which closely matches the sensitivity analysis prediction.

From Fig. 5 the values of the rms errors are comparable with the values measured by Prasad and Adrian[1] for the case of an equivalent ($\theta = 16°$) translation stereocamera. The only difference is that the rms error $\sigma_{\Delta y}$ in Fig. 5 is somewhat larger than $\sigma_{\Delta x}$. We believe that this may be due to the imperfect matching of the two views, i.e., this may be a manifestation of the registration error described by Prasad and Adrian.[1] The fact that the views are distorted owing to nonuniform magnification makes the registration process more difficult. Therefore, whereas the angular-displacement camera theoretically allows much higher values of θ (and therefore better out-of-plane accuracy) than the translation system, the benefit can be achieved only after accurate registration.

4. Conclusions

We have investigated the performance of Scheimpflug stereocamera PIV. Computer error analysis showed that the system accuracy was influenced strongly by the off-axis angle θ. We conducted a uniform translation test for this system. Computer error analysis predicted an out-of-plane error versus in-plane error ratio $\sigma_{\Delta z}/\sigma_{\Delta x}$ of approximately 2.8; uniform translation experiments gave a value of 3.5. Moreover, experimental results indicate that this system can provide an accuracy comparable with the translation stereocamera system. Even higher accuracies should be possible at larger values of θ.

Appendix A: Error Analysis of Scheimpflug Stereocamera Equations

$$\frac{\sigma_{\Delta x}^{\,2}}{\sigma_{\Delta X}^{\,2}} = \left\{\frac{\dfrac{\Delta X_2 d_1 \Theta_{21}}{cos(\theta) A_1} + \Theta_{21} A_5}{A_3} - \frac{\left[\dfrac{\Delta X_2 d_1 A_4}{\cos(\theta) A_1} - \dfrac{\Delta X_1 d_1 A_5}{\cos(\theta) A_2}\right]\Theta_{21}}{A_3^{\,2}}\right\}^2 + \left\{\frac{\dfrac{\Delta X_1 d_1 \Theta_{12}}{\cos(\theta) A_2} + \Theta_{12} A_4}{A_3} + \frac{\left[\dfrac{\Delta X_1 d_1 A_5}{\cos(\theta) A_2} - \dfrac{\Delta X_2 d_1 A_4}{\cos(\theta) A_1}\right]\Theta_{12}}{A_3^{\,2}}\right\}^2,$$

where

$$A_1 = 2\Delta X_2 \sin(\theta) + \frac{d_1}{\cos(\theta)},$$

$$A_2 = 2\Delta X_1 \sin(\theta) + \frac{d_1}{\cos(\theta)},$$

$$A_3 = 2\tan(\theta) d_1 - \frac{\Delta X_1 d_1}{\cos(\theta) A_2} + \frac{\Delta X_2 d_1}{\cos(\theta) A_1},$$

$$A_4 = \tan(\theta) d_1 - \frac{\Delta X_1 d_1}{\cos(\theta) A_2},$$

$$A_5 = -\tan(\theta) d_1 - \frac{\Delta X_2 d_1}{\cos(\theta) A_1},$$

$$\Theta_{ij} = \frac{2\Delta X_j d_1 \sin(\theta)}{\cos(\theta) A_i^{\,2}} - \frac{d_1}{\cos(\theta) A_i}.$$

$$\frac{\sigma_{\Delta y}^{\,2}}{\sigma_{\Delta X}^{\,2}} = (\Phi_{12} B_5)^2 + (\Phi_{21} B_5)^2 + \frac{B_4^{\,2}}{B_3} + \left[\frac{2\tan(\theta) d_1}{B_3^{\,2}}\right]^2,$$

where

$$B_1 = 2\Delta X_2 \sin(\theta) + \frac{d_1}{\cos(\theta)},$$

$$B_2 = 2\Delta X_1 \sin(\theta) + \frac{d_1}{\cos(\theta)},$$

$$B_3 = 2\tan(\theta) d_1 - \frac{\Delta X_1 d_1}{\cos(\theta) B_2} + \frac{\Delta X_2 d_1}{\cos(\theta) B_1},$$

$$B_4 = \frac{-\Delta X_1 d_1}{\cos(\theta) B_2} + \frac{\Delta X_2 d_1}{\cos(\theta) B_1},$$

$$B_5 = \frac{2\tan(\theta) d_1}{B_3}\left(\frac{\Delta Y_1 + \Delta Y_2}{B_3}\right),$$

$$\Phi_{ij} = \frac{1}{2}\left[\frac{2\Delta X_i d_1 \tan(\theta)}{B_j^{\,2}} - \frac{d_1}{\cos(\theta) B_j}\right].$$

$$\frac{\sigma_{\Delta z}^{\,2}}{\sigma_{\Delta X}^{\,2}} = \left(\frac{\prod_{12}}{C_3} - \frac{C_4 \prod_{12}}{C_3^{\,2}}\right)^2 + \left(\frac{\prod_{21}}{C_3} - \frac{C_4 \prod_{21}}{C_3^{\,2}}\right)^2,$$

where

$$C_1 = 2\Delta X_2 \sin(\theta) + \frac{d_1}{\cos(\theta)},$$

$$C_2 = 2\Delta X_1 \sin(\theta) + \frac{d_1}{\cos(\theta)},$$

$$C_3 = 2\tan(\theta) d_1 - \frac{\Delta X_1 d_1}{\cos(\theta) C_2} + \frac{\Delta X_2 d_1}{\cos(\theta) C_1},$$

$$C_4 = \frac{-\Delta X_1 d_1}{\cos(\theta) C_2} + \frac{\Delta X_2 d_1}{\cos(\theta) C_1},$$

$$\prod_{ij} = d_1 \left[\frac{2\Delta X_i d_1 \tan(\theta)}{C_j^{\,2}} - \frac{d_1}{\cos(\theta) C_j} \right].$$

We thank NASA Langley for supporting this research under contract NAG 1 1815.

References

1. A. K. Prasad and R. J. Adrian, "Stereoscopic particle image velocimetry applied to liquid flows," Exp. Fluids **15,** 49–60 (1993).
2. A. K. Prasad and K. Jensen, "Scheimpflug stereocamera for particle image velocimetry in liquid flows," Appl. Opt. **34,** 7092–7099 (1995).
3. R. E. Altenhofen, "Rectification," in *Manual of Photogrammetry* (American Society of Photogrammetry, Washington, D.C., 1952), p. 457.
4. A. K. Prasad, R. J. Adrian, C. C. Landreth, and P. W. Offutt, "Effect of resolution on the speed and accuracy of particle image velocimetry interrogation," Exp. Fluids **13,** 105–116 (1992).
5. A. Boillot and A. K. Prasad, "Optimization procedure for pulse separation in cross-correlation PIV," Exp. Fluids **21,** 87–93 (1996).
6. R. J. Adrian, "Particle-imaging techniques for experimental fluid mechanics," Ann. Rev. Fluid Mech. **23,** 261–304 (1991).